Title

Reduced glucose uptake and Aβ in brain regions with hyperintensities in connected white matter

Authors

Glodzik, L
Kuceyeski, A
Rusinek, H
et al.

Publication Date

2014-10-01

DOI

10.1016/j.neuroimage.2014.06.060

Peer reviewed

HHS Public Access

Author manuscript

Neuroimage. Author manuscript; available in PMC 2015 October 15.

Published in final edited form as:

Neuroimage. 2014 October 15; 100: 684–691. doi:10.1016/j.neuroimage.2014.06.060.

Reduced glucose uptake and Aβ in brain regions with hyperintensities in connected white matter

L. Glodzik, MD, PhD[#1,2], **A. Kuceyeski, PhD**[#†,3], **H. Rusinek, PhD**[2], **W. Tsui, MS**[1], **L. Mosconi, PhD**[1], **Y. Li, MD**[1], **R.S. Osorio, MD**[1], **S. Williams, RN**[1], **C. Randall, MA**[1], **N. Spector, BA**[1], **P. McHugh, MD**[1], **J. Murray, BS**[1], **E. Pirraglia, MA**[1], **S. Vallabhajosula, PhD**[3], **A. Raj, PhD**[3], and **M.J. de Leon, EdD**[1]

[1]Center for Brain Health, Department of Psychiatry, New York University School of Medicine, New York, USA

[2]Department of Radiology, New York University School of Medicine, New York, USA

[3]Department of Radiology and Brain and Mind Research Institute, Weill Cornell Medical College, New York, USA

[#] These authors contributed equally to this work.

Abstract

Interstitial concentration of amyloid beta (Aß) is positively related to synaptic activity in animal experiments. In humans, Aß deposition in Alzheimer's disease overlaps with cortical regions highly active earlier in life. White matter lesions (WML) disrupt connections between gray matter (GM) regions which in turn changes their activation patterns. Here, we tested if WML are related to Aß accumulation (measured with PiB-PET) and glucose uptake (measured with FDGPET) in connected GM. WML masks from 72 cognitively normal (age 61.7±9.6 years, 71% women) individuals were obtained from T2-FLAIR. MRI and PET images were normalized into common space, segmented and parcellated into gray matter (GM) regions. The effects of WML on connected GM regions were assessed using the Change in Connectivity (ChaCo) score. Defined for each GM region, ChaCo is the percentage of WM tracts connecting to that region that pass through the WML mask. The regional relationship between ChaCo, glucose uptake and Aß was explored via linear regression. Subcortical regions of the bilateral caudate, putamen, calcarine,

[†]Corresponding author information: Amy Kuceyeski Address: 525 East 71st St, S-125, New York, NY 11065 Phone: (212)-746-5439 amk2012@med.cornell.edu.

Disclosure of Conflicts

We would like to disclose the following possible conflicts. Dr. Glodzik was a PI on an Investigator Initiated project funded by Forest Laboratories, Inc., and received a travel grant from Roche Pharma. Drs. Mosconi, Tsui and de Leon have a patent on a technology that was licensed to Abiant Imaging Inc. by NYU and, as such, have a financial interest in this license agreement and hold stock and stock options on the company. Drs. Mosconi and de Leon have received compensation for consulting services from Abiant Imaging. Dr. de Leon has received personal compensation for serving as a consultant for Abiant Imaging Inc. (Chicago, IL). He was also a PI on a completed Investigator Initiated project funded by Forest Laboratories, Inc., and a completed clinical trial supported by Neuroptix (Boston). Dr. de Leon received travel expenses for serving on the French Alzheimer Disease Foundation and an honorarium as a consultant to Roche Pharma. Dr. Raj receives research support from EMD Serono and Biogen Idec.

insula, thalamus and anterior cingulum had WM connections with the most lesions, followed by frontal, occipital, temporal, parietal and cerebellar regions. Regional analysis revealed that GM with more lesions in connecting WM and thus impaired connectivity had lower FDG-PET ($r=0.20$, $p<0.05$ corrected) and lower PiB uptake ($r=0.28$, $p<0.05$ corrected). Regional regression also revealed that both ChaCo ($\beta=0.045$) and FDG-PET ($\beta=0.089$) were significant predictors of PiB. In conclusion, brain regions with more lesions in connecting WM had lower glucose metabolism and lower Aß deposition.

Keywords

Magnetic Resonance Imaging; Positron Emission Tomography; amyloid beta; aging; cerebrovascular disorders

1. Introduction

Animal experiments show that interstitial concentration of amyloid beta (Aß) increases with synaptic activity [Bero et al., 2011; Cirrito et al., 2005]. Diurnal fluctuation of cerebrospinal fluid Aß42 in humans peaks in the evening and decreases at night, supporting a relationship to neuronal activity [Kang et al., 2009]. Imaging techniques have shown that the highly active heteromodal association cortices in healthy subjects spatially overlap with patterns of Aß deposition in patients with Alzheimer's disease. A hypothesis has therefore been proposed that states regions with high levels of connectivity and cortical activation throughout the life span may be more prone to greater Aß burden [Buckner et al., 2009; Jagust and Mormino, 2011].

White matter (WM) tracts interconnect gray matter (GM) areas allowing propagation of activation from one cortical region to another [Filley, 2010]. White matter lesions (WML) manifesting as areas of hyperintense signal on MRI images are, alongside brain atrophy, the most common pathological findings associated with aging [de Leeuw et al., 2001]. Regardless of the mechanism, which is debated [Scarpelli et al., 1994; Scheltens et al., 1995], WML indicate a disruption of normal pattern of brain connections, and have been linked to metabolic changes in distal areas and clinical symptoms [DeCarli et al., 1995; Nordahl et al., 2006].

Here we test the following hypothesis: Aß load and glucose metabolism in a given cortical region is inversely related to the amount of connecting WM fibers with hyperintensities. Although relationships between measures of WML burden, glucose metabolism and Aß accumulation have been previously reported [DeCarli et al., 1995; Hedden et al., 2012; Kuczynski et al., 2008; Marchant et al., 2012; Provenzano et al., 2013; Reed et al., 2004; Sultzer et al., 2002; Tullberg et al., 2004], none consider the topology of the WM fiber network. In this study, we examine relationships between WM connectivity disruption and fluorodeoxyglucose (FDG) uptake and Pittsburgh compound B (PiB) deposition on a region-wise basis.

2. Materials and Methods

2.1 Subjects

Seventy-two subjects were studied (mean age 61.7±9.6 years, 71% women, education17±1.9 years). All were recruited in the Center for Brain Health New York University School of Medicine, and signed IRB approved consents for protocols investigating risk factors of cognitive decline and Alzheimer's disease. The clinical evaluation included an interview according to the Brief Cognitive Rating Scale and rating on Global Deterioration Scale [Reisberg et al., 1993]. Based on clinical assessment, all subjects were diagnosed as cognitively healthy: with (Global Deterioration Scale of 2) or without subjective memory complaints (Global Deterioration Scale of 1), but not fulfilling the criteria for mild cognitive impairment or dementia. Subjects scoring>16 on the 17-item Hamilton Depression Scale were excluded [Bech et al., 1986]. All subjects had≥26 points on Mini Mental State Examination [Folstein, 1983]. Subjects with brain pathology (tumor, neocortical infarction), diabetes, axis I disorders and those using psychoactive medications were also excluded.

Standard Approvals, Registrations, and Patient Consents—A statement of written informed consent for participation in a study of longitudinal changes in brain aging was obtained from all patients participating in the study.

2.2 Imaging

MRI acquisition—Imaging was performed on a 1.5 T GE scanner (GE, Milwaukee, WI, USA). All participants received T1-weighted and FLAIR scans. T1 weighted (gradient echo) MRI scans were acquired in the coronal orientation (repetition time=35 ms, time to echo=2 ms, flip angle=60°, number of excitations=1, slice thickness=1.6 mm, field of view=200 mm, matrix=256×192 ×124, reconstructed as 256 × 256). FLAIR images were acquired in the axial orientation with repetition time=9279 ms, time to echo=127 ms, time to inversion=2300 ms, flip angle=90°, number of excitations=1, slice thickness=3.3 mm, field of view=240 mm, matrix=256×192, as 256 × 256 images).

WML segmentation—WML and whole brain volumes were determined using a locally developed software package *FireVoxel* (https://files.nyu.edu/hr18/public). Brain parenchyma volume, V_B, was obtained by automatic segmentation of T1 weighted images [Mikheev et al., 2008] and the WML masks were obtained from FLAIR images, which had been corrected for signal nonuniformity with N3 algorithm [Sled et al., 1998]. The WML mask was created via the following process. A “pure WM” seed, defined as the 1-cm^3 region where the coefficient of variability of signal is minimal, was identified. An initial mask M_0 was then constructed from voxels with signal > 0.55 relative to the seed signal (cerebrospinal fluid spaces are excluded from further consideration). Subvoxel erosion with radius 2.7 mm was then applied to the mask M_0 to disconnect the head/neck muscles and optic nerves. The program then computed the largest connected components of the eroded mask. A constrained growth operator was applied to generate the brain parenchyma mask M. The brain stem, the pons and the cerebellum were retained in M. Subsequently, a set M' was then constructed by applying the 3D morphologic fill operator to M. This was done to assure that all hypointensities located at the ventricular border were considered. In the next step, we

constructed the set L_0 of voxels in M' with signal above 2.5 standard deviations above the mean FLAIR signal for M. This set was than filtered to remove: (a) cortical voxels, defined as those located within 3 mm of the surface of M; (b) small clusters of volume<12 mm^3; and (c) connected regions having>50% CSF border. The result of automatic 3 mm erosion in step (a) was inspected and edited if needed.

WML volume V_{WML} was then calculated as the product of FLAIR voxel volume and the number of WML voxels. The fractional WML volume (fV_{WML}) was generated as V_{WML}/V_B. FLAIR MR-images were spatially normalized to MNI (Montreal Neurological Institute) space using SPM, and the resulting non-linear transformation was applied to the WML mask (with nearest neighbor interpolation). Coregistrations were checked visually for accuracy.

FDG-PET and PiB-PET acquisition—Scans were performed an LS Discovery scanner; G.E. Medical Systems, Milwaukee, WI; 5.4 mm full width at half maximum, 30 cm field of view. Before the scanning a venous line was inserted in the antecubital vein, and subjects rested in the quiet and dim room. PiB-PET scanning started about 60 minutes after isotope injection and lasted 30 minutes. In each case, 15 mCi (~550 MBq) of N-methyl(11C)2-(4'-methylaminophenyl)-6-hydroxy-benzothiazole (PiB; radiochemical purity>98%) was administered. The FDG scan procedure started 30 minutes after completion of the PiB scan or on a separate day. After an overnight fast, subjects were injected with 5 mCi (~340 MBq) of 2-(^{18}F)fluoro-2-Deoxy-D-glucose, positioned in the scanner approximately 35 min after injection, and scanned for 20 minutes. Prior to each PET examination, a 5 min CT transmission scan was acquired for attenuation correction. All images were corrected for photon attenuation, scatter, and radioactive decay, and reconstructed into a 512x512 matrix using iterative algorithms: LS Discovery: FORE IT, Fourier rebinning followed by Order Subset Expectation Maximization, OSEM, 8 iterations, 16 subsets, 3.375 mm voxel.

PiB-PET image processing—The 60-90 min PiB and the 40-60 min of FDG data were used to generate summed PET images. They were coregistered to their corresponding T1-MRI using Statistical Parametric Mapping (SPM, version 8) [Ashburner and Friston, 2000]. The parameters obtained from normalization of T1-MRI images to the MNI space were then applied to the FDGPET and PiB-PET images to reslice them into common space. An automated cerebellar region of interest (ROI) was used to extract the cerebellar intensity value [Li et al., 2008]. The cerebellar intensity value was then applied to create intensity ratios images for both type of PET images, by normalizing each voxel to the cerebellum through image calculation function. Cerebellar ratio images were then used in all further analyses.

The average signal for cortical and subcortical GM regions was calculated for both PiB-PET and FDG-PET images. The GM regions were defined by identifying voxels within SPM's MNI space GM tissue mask and then assigning each to one of the 116-regions in the MNI space Automated Anatomical Labeling atlas [Tzourio-Mazoyer et al., 2002], and applying that same regional definition to each individual's MNI space PiB-PET and FDG-PET images so that the region assignments were uniform for all subjects. Proximity to WMLs may also affect the function and/or PiB deposition in a GM region. Therefore, the white matter distance (WMD) was defined for each of the 116 regions as the average distance to WML. It

was calculated by taking the mean of the Euclidean distance of each region's center of mass to each voxel in the WML mask.

2.2 The NeMo Tool

The NeMo Tool [Kuceyeski et al., 2013] was used to estimate regional and global structural connectivity changes that may result from a given WM abnormality mask. The NeMo tool is based on the Tractogram Reference Set, which is a large set of WM streamlines created using probabilistic tractography in 72 normal controls (independent of this study group). These streamlines are used to project given WM abnormalities onto structurally "connected" GM regions. The NeMo tool reports connectivity changes in two ways: 1) local Change in Connectivity (ChaCo) scores that were based on a 116 region atlas and 2) global network changes based on graph theoretical metrics, i.e. efficiency and characteristic path length. Both of these graph metrics quantify how easily information flows within a network; for example if a signal moves more easily from node to node within a network then it will have larger efficiency and smaller characteristic path length. In the work presented here, the lesion masks were binary so ChaCo scores were simply the percent of tracts ending in a given GM region that pass through abnormal WML out of the total number of tracts connecting to that GM region. ChaCo scores were presented as negative values, indicating that the implied influence of the WML was that of disruption. This means that lower (more negative) values indicate more connectivity disruption and larger (more positive) values indicate less connectivity disruption.

2.3 Statistical Approach

The relationship between lesions in connecting WM, Aß deposition, glucose metabolism, and proximity to WMLs were explored on an individual subject, region-wise basis. Because we were interested in the effect of WM connectivity disruption, only the 5% most disrupted regions over the population (out of 72×116 regions) were retained in the following analysis. Thresholding was done on an individual region-wise basis, i.e. scores were not averaged before thresholding. We chose the top 5% most disrupted (regions with ChaCo<-1.67%) as the ChaCo scores were quite minimal over the population and this threshold assures that we are taking only the regions that had the most lesions in connecting WM without excluding too many data points. If we included more regions, the ChaCo scores would be greater than -1% and may be subject to noise effects. On the other hand, if the cutoff was made more stringent, the number of included data would shrink and the resulting analysis would have too small a number of data points to draw conclusions. In order to verify that the particular choice of cutoff did not unduly influence the overall results, we doubled and halved the chosen threshold of 5% and compared the regression model results.

Before and after thesholding, the ChaCo scores appeared to be exponentially distributed and were transformed before performing statistical analysis that assumes Gaussianity. A resampling scheme used previously [Honey et al., 2009] was implemented. We drew N samples from a standard Gaussian distribution ($\mu=0$, $\sigma=1$), where N was the number of elements in the thresholded ChaCo scores. We replaced the most negative ChaCo score with the smallest normal value, the second most negative ChaCo score with the second-smallest normal value and so on until all ChaCo scores have been replaced with a normal value.

Smaller values of the transformed ChaCo still indicate more disconnection, as in the original scores.

Pearson's correlations were calculated between all of the regional metrics and their significance was assessed using Bonferroni correction for multiple comparisons ($p<0.05/6=0.0083$). The inter-relationship of each of these values with Aß deposition was further explored via linear regression [Draper and Smith, 1998]. PiB was the dependent variable; FDG-PET, WMD, and transformed ChaCo scores were the independent predictors.

3. Results

The mean fV_{WML} was .37%±.41% (median .33%, interquartile range .22%, min .01%, max 2.5%). The ChaCo scores varied across the population – Figure 1 shows the lesion masks and the corresponding ChaCo scores for three different individuals via the glassbrain display. The glassbrain display depicts each region as a sphere, where the size is proportional to the ChaCo score and the color denotes regional (cortical lobe and subcortical) membership. The mean ChaCo score over the population for each GM region is displayed via the glassbrain in Figure 2, and a boxplot of the distribution of scores over the population are given in the bottom part of Figure 2. Each boxplot depicts the distribution of scores for a particular region, color-coded with the same key as the glassbrain. Regions of the bilateral caudate, putamen, calcarine, anterior cingulum, lingual gyri and thalamus were the most affected (had the highest mean ChaCo scores), followed by other occipital, frontal, parietal, and temporal regions.

Regions that were included in the correlation/regression analysis (top 5% of ChaCo scores) coincided largely with those that had highest mean ChaCo scores, unsurprisingly. Sixty-eight of the 72 individuals had at least one region included, and 52/90 cortical and subcortical regions were represented (none of the 26 cerebellar regions were included). Significant correlations existed among all four variables (ChaCo, FDG-PET, PIB-PET, and WMD) after Bonferroni correction for multiple comparisons. Figure 3 shows scatter plots of each of the variables against the other (in the off-diagonal plots), in addition to histograms of each variable (in the diagonal plots). However, correlations between transformed ChaCo and FDG-PET ($r=0.20$, $p<0.0083$) and PiB-PET ($r=0.28$, $p<0.0083$) were higher than correlations between WMD and FDG-PET ($r=0.16$, $p<0.0083$) and PiB-PET ($r=0.14$, $p<0.0083$). The highest correlations existed between PiB-PET and FDG-PET ($r=0.44$, $p<0.0083$). We inspected the correlation between PiB-PET and FDG-PET in cortical and subcortical regions with no lesions in connecting WM (ChaCo scores of 0), to be sure that the positive relationship found was not due to the thresholding of ChaCo scores. The correlation in these regions was still positive ($r = 0.20$, $p < 0.0013$), although about half what was found in regions with some disconnection. We would also like to point out that the non-parametric Spearman correlations of the original untransformed ChaCo scores with the other regional imaging variables (see Supplemental Table 1) were very similar to the Pearson correlations with the transformed ChaCo scores. Therefore we believe that the underlying relationships of the variables were not fundamentally changed by this transform.

The final linear regression model (R^2=0.23) indicated that both FDG-PET and transformed ChaCo had positive relationships with PiB deposition (Figure 4, top). The coefficient with the smallest p-value (5.2×10^{-18}) was FDG-PET, which was positively associated with PiB (β=0.089±0.0099), (see Figure 4, bottom left). Transformed ChaCo was also included in the final model ($p=4.6\times10^{-6}$), and the coefficient indicated a positive relationship to PiB (β=0.045±0.0099, Figure 4 bottom right). The same regression analysis was performed with the top 2.5% and 10% most disconnected regions, and the results were very similar. FDG-PET and transformed ChaCo were the only two significant contributors to each model, and they both had positive regression coefficients. In the model containing the top 2.5% most disconnected regions, the regression coefficients were: FDG-PET (0.11±0.013) and ChaCo (0.044±0.013). In the model that included the top 10% most disconnected regions, the regression coefficients were: FDG-PET (0.079±0.0071 and ChaCo (0.021±0.0071).

4. Discussion

Cognitively normal elderly subjects with WML had implied connectivity loss mostly in subcortical regions, particularly the caudate nucleus. Frontal and occipital lobes had some disconnection as well, with the temporal and parietal showing little and the cerebellum showing no disruptions in connection. Most importantly, when examined on region to region basis, the correlations between ChaCo, FDG-PET and PiB-PET indicate that regions with more lesions in connecting WM have less glucose metabolism and lower Aß deposition. A weaker relationship was also found between WMD; GM regions closer to WMLs tended to have lower glucose consumption and lower Aß levels.

One simple explanation for our finding is that changes in the vasculature supplying connected WM and GM regions might have caused hypoperfusion resulting both in WML and reduction in cortical metabolism. However, other explanations are also plausible. Since implied connectivity loss was associated with lower glucose metabolism and lower Aß in connecting regions, we posit that WML lesions are causing disruption of incoming and/or outgoing electrical signals to that region, which in turn lowers synaptic activity and (therefore?) Aß deposition. Loss of synapses could also explain our findings. Alternatively, regions with some neuronal loss may have associated hyperintensities in their connecting WM tracts. This analysis cannot determine the direction of the relationships between the dependent and independent variables, but only that one exists.

Glucose consumption explains some of the variance in regional Aß concentration; however, the ChaCo score was also a significant predictor in the regression model. WMD was not included in the final model, suggesting that the ChaCo score is indeed capturing something other than proximity, namely, the topology of the brain network. Furthermore, we speculate that if WM connectivity disruption measured by the ChaCo score affected the Aß deposition only through a decrease in activity due to lower signal input from the rest of the brain, we would assume that the final model would only include FDG-PET. However, the ChaCo score was a significant predictor of PiB, suggesting that there may be another effect of WM disruption apart from an associated decrease in glucose consumption. It has recently been shown that Aß as well as other misfolded disease proteins may propagate via transsynaptic spread [Frost et al., 2009; Palop and Mucke, 2010]. This “prion-like” mechanism was the

basis for a theoretical model of dementia progression that was validated using actual patient data [Raj et al., 2012]. Our results agree with these findings in that they suggest disruption in WM connections via lesions may prevent the spread of Aß to the connected GM regions.

Our results are in line with previous studies which revealed negative relationships between measures of WML volume and global [Kochunov et al., 2009] and regional (mostly frontal) glucose metabolism [DeCarli et al., 1995; Kuczynski et al., 2008; Reed et al., 2004; Sultzer et al., 2002; Tullberg et al., 2004]. With regard to the PIB/WML relationship an interesting picture emerges. It is acknowledged that vascular disease contributes to Alzheimer's disease pathology [Zlokovic, 2011]. This view stimulated a breadth of studies that examined the connections between WML (as a manifestation of vascular pathology) and Aß accumulation measured with PiB-PET. Interestingly, only some showed that more WML translated into more PIB deposition [Grimmer et al., 2012], but most of them did not show such relationships [Hedden et al., 2012; Marchant et al., 2012; Provenzano et al., 2013]. We posit that the disconnection hypothesis can explain these findings: WMLs cause disruption of WM tracts, diminish input from damaged fibers, and result in lower PIB deposition.

Current literature is anything but conclusive on correlations (or lack thereof) between PiB and FDG-PET imaging biomarkers. Study results vary from finding a lack of correlation [Carter et al., 2012; Furst et al., 2012; Li et al., 2008; Yokokura et al., 2011], negative correlation [Drzezga et al., 2008; Edison et al., 2007; Klunk et al., 2004], or, as observed here, positive cross-sectional [Cohen et al., 2009; Oh et al., 2014] or longitudinal [Förster et al., 2012] correlation. We believe there are likely a few different factors that can explain these apparent discrepancies, which we expand upon in the following paragraphs.

First, the diagnostic group plays an important role. Some earlier publications indeed indicated a negative correlation between PiB retention and FDG uptake in AD patients, predominantly in parietal and temporal regions where typical abnormalities overlap, but not frontal regions [Edison et al., 2007; Klunk et al., 2004] where they do not overlap. Another example is in sematic dementia, where patients exhibited pronounced reduction in glucose uptake of temporal regions that was not accompanied by amyloid deposition [Drzezga et al., 2008]. Still others have reported comparable and widespread PIB accumulation in AD and posterior cortical atrophy, but different hypometabolism patterns in these two conditions [Rosenbloom et al., 2011]. Therefore, in our opinion, the quite common notion that amyloid accumulation equals hypometabolism, or that it is a reason for hypometabolism, must be taken with caution. Second, most previous studies do not examine relationships of PiB and FDG-PET on a smaller region-by-region basis. Rather, they mostly focus on larger regions important to disease-specific pathology, encompassing many different non-overlapping areas, or were reported between global PiB index and regional FDG uptake. In our study, we presented relationships bases on individual AAL regions.

Finally, although the largest study to date of cognitively healthy elderly reported a negative correlation between amyloid deposition and glucose metabolism [Lowe et al., 2014], these relationships were predominantly seen in AD-related regions and were therefore parallel to previous observations in AD patients. Moreover, subjects in this study were on average 16 years older than our group, thus likely to have more advanced AD processes. Given this

context, we offer that their findings may still indicate regional overlap of possibly independent pathologies. In fact, others have found that cognitively healthy elderly manifest increases of both glucose metabolism and amyloid deposition in overlapping brain regions [Oh et al., 2014]. Additionally, in early AD, longitudinal increase in amyloid deposition was observed in regions were baseline metabolism was preserved, or only mildly reduced[Förster et al., 2012], further supporting the concept that metabolic activity may be associated with amyloid deposition.

Limitations of our study include lack of partial volume correction. Conceivably, disruption of connections by WML could have caused atrophy in related gray matter regions. This might have decreased both FDG uptake and PIB retention. Neuropathological validation of diminished input from damaged fibers is also missing. Moreover our study cohort presented relatively low level of vascular pathology as evidenced by fV_{WML} and ChaCo values near zero in cortical regions. Another limitation of the study arises from the use of tractography - a complex and noisy process even in normal subjects. There is currently no method that can fully capture true underlying anatomy; e.g. probabilistic tractography used in the NeMo Tool deduces fibers that are not always reproducible and has difficulty constructing long-range connections. In addition, there is natural variability in WM connections due to external and internal factors. As a result, the individual normal tractograms in NeMo tool may not be accurately representing a particular individual's connectivity. However, the fact that ChaCo scores are averaged over a large number of normal subjects' tractograms should account for both natural variability and noise in image processing.

In conclusion, the implied disruption of connections resulting from the presence of WML in a group of cognitively normal elderly adults was related to reduced glucose uptake and Aß deposition within connecting GM regions. This indirectly supports the hypothesis linking Aß accumulation to activity level within cortical areas. More importantly, our findings suggested yet another mechanism for reduced Aß: that of WM connectivity disruption and a hindrance of the pathways that enable delivery of the misfolded protein. Longitudinal studies with more diverse population are warranted to confirm our observation.

Supplementary Material

Refer to Web version on PubMed Central for supplementary material.

Acknowledgements

This work was supported by a Leon Levy Foundation Neuroscience Fellowship and the following NIH grants: P41 RR023953-02, P41 RR023953-02S1, R01 NS075425, 2R01AG013616-22, R01-AG035137, RC2-AG036502, P30 AG008051 and HL111724-01.

References

Ashburner J, Friston KJ. Voxel-based morphometry--the methods. Neuroimage. 2000; 11:805–21. [PubMed: 10860804]

Bech P, Kastrup M, Rafaelsen OJ. Mini-compendium of rating scales for states of anxiety depression mania schizophrenia with corresponding DSM-III syndromes. Acta Psychiatr Scand Suppl. 1986; 326:1–37. [PubMed: 3458353]

Bero AW, Yan P, Roh JH, Cirrito JR, Stewart FR, Raichle ME, Lee J-M, Holtzman DM. Neuronal activity regulates the regional vulnerability to amyloid-β deposition. Nat Neurosci. 2011; 14:750–6. [PubMed: 21532579]

Buckner RL, Sepulcre J, Talukdar T, Krienen FM, Liu H, Hedden T, Andrews-Hanna JR, Sperling RA, Johnson KA. Cortical hubs revealed by intrinsic functional connectivity: mapping, assessment of stability, and relation to Alzheimer's disease. J Neurosci. 2009; 29:1860–73. [PubMed: 19211893]

Carter SF, Schöll M, Almkvist O, Wall A, Engler H, Långström B, Nordberg A. Evidence for astrocytosis in prodromal Alzheimer disease provided by 11C-deuterium-L-deprenyl: a multitracer PET paradigm combining 11C-Pittsburgh compound B and 18F FDG. J Nucl Med. 2012; 53:37–46. [PubMed: 22213821]

Cirrito JR, Yamada KA, Finn MB, Sloviter RS, Bales KR, May PC, Schoepp DD, Paul SM, Mennerick S, Holtzman DM. Synaptic activity regulates interstitial fluid amyloid-beta levels in vivo. Neuron. 2005; 48:913–22. [PubMed: 16364896]

Cohen AD, Price JC, Weissfeld LA, James J, Rosario BL, Bi W, Nebes RD, Saxton JA, Snitz BE, Aizenstein HA, Wolk DA, Dekosky ST, Mathis CA, Klunk WE. Basal cerebral metabolism may modulate the cognitive effects of Abeta in mild cognitive impairment: an example of brain reserve. J Neurosci. 2009; 29:14770–8. [PubMed: 19940172]

DeCarli C, Murphy DG, Tranh M, Grady CL, Haxby JV, Gillette JA, Salerno JA, Gonzales-Aviles A, Horwitz B, Rapoport SI. The effect of white matter hyperintensity volume on brain structure, cognitive performance, and cerebral metabolism of glucose in 51 healthy adults. Neurology. 1995; 45:2077–84. [PubMed: 7501162]

Draper, NR.; Smith, H. Applied Regression Analysis (Wiley Series in Probability and Statistics). Wiley-Interscience; 1998.

Drzezga A, Grimmer T, Henriksen G, Stangier I, Perneczky R, Diehl-Schmid J, Mathis CA, Klunk WE, Price J, DeKosky S, Wester H-J, Schwaiger M, Kurz A. Imaging of amyloid plaques and cerebral glucose metabolism in semantic dementia and Alzheimer's disease. Neuroimage. 2008; 39:619–33. [PubMed: 17962045]

Edison P, Archer HA, Hinz R, Hammers A, Pavese N, Tai YF, Hotton G, Cutler D, Fox N, Kennedy A, Rossor M, Brooks DJ. Amyloid, hypometabolism, and cognition in Alzheimer disease: an [11C]PIB and [18F]FDG PET study. Neurology. 2007; 68:501–8. [PubMed: 17065593]

Filley CM. White matter: organization and functional relevance. Neuropsychol Rev. 2010; 20:158–73. [PubMed: 20352350]

Folstein MF. The Mini-Mental State Examination. Arch Gen Psychiatry. 1983; 40:812. [PubMed: 6860082]

Förster S, Grimmer T, Miederer I, Henriksen G, Yousefi BH, Graner P, Wester H-J, Förstl H, Kurz A, Dickerson BC, Bartenstein P, Drzezga A. Regional expansion of hypometabolism in Alzheimer's disease follows amyloid deposition with temporal delay. Biol Psychiatry. 2012; 71:792–7. [PubMed: 21679929]

Frost B, Ollesch J, Wille H, Diamond MI. Conformational diversity of wild-type Tau fibrils specified by templated conformation change. J Biol Chem. 2009; 284:3546–51. [PubMed: 19010781]

Furst AJ, Rabinovici GD, Rostomian AH, Steed T, Alkalay A, Racine C, Miller BL, Jagust WJ. Cognition, glucose metabolism and amyloid burden in Alzheimer's disease. Neurobiol Aging. 2012; 33:215–25. [PubMed: 20417582]

Grimmer T, Faust M, Auer F, Alexopoulos P, Förstl H, Henriksen G, Perneczky R, Sorg C, Yousefi BH, Drzezga A, Kurz A. White matter hyperintensities predict amyloid increase in Alzheimer's disease. Neurobiol Aging. 2012; 33:2766–73. [PubMed: 22410648]

Hedden T, Mormino EC, Amariglio RE, Younger AP, Schultz AP, Becker JA, Buckner RL, Johnson KA, Sperling RA, Rentz DM. Cognitive profile of amyloid burden and white matter hyperintensities in cognitively normal older adults. J Neurosci. 2012; 32:16233–42. [PubMed: 23152607]

Honey CJ, Sporns O, Cammoun L, Gigandet X, Thiran JP, Meuli R, Hagmann P. Predicting human resting-state functional connectivity from structural connectivity. Proc Natl Acad Sci U S A. 2009; 106:2035–40. [PubMed: 19188601]

Jagust WJ, Mormino EC. Lifespan brain activity, β-amyloid, and Alzheimer's disease. Trends Cogn Sci. 2011; 15:520–6. [PubMed: 21983147]

Kang J-E, Lim MM, Bateman RJ, Lee JJ, Smyth LP, Cirrito JR, Fujiki N, Nishino S, Holtzman DM. Amyloid-beta dynamics are regulated by orexin and the sleep-wake cycle. Science. 2009; 326:1005–7. [PubMed: 19779148]

Klunk WE, Engler H, Nordberg A, Wang Y, Blomqvist G, Holt DP, Bergström M, Savitcheva I, Huang G, Estrada S, Ausén B, Debnath ML, Barletta J, Price JC, Sandell J, Lopresti BJ, Wall A, Koivisto P, Antoni G, Mathis CA, Långström B. Imaging brain amyloid in Alzheimer's disease with Pittsburgh Compound-B. Ann Neurol. 2004; 55:306–19. [PubMed: 14991808]

Kochunov P, Ramage AE, Lancaster JL, Robin DA, Narayana S, Coyle T, Royall DR, Fox P. Loss of cerebral white matter structural integrity tracks the gray matter metabolic decline in normal aging. Neuroimage. 2009; 45:17–28. [PubMed: 19095067]

Kuceyeski A, Maruta J, Relkin N, Raj A. The Network Modification (NeMo) Tool: elucidating the effect of white matter integrity changes on cortical and subcortical structural connectivity. Brain Connect. 2013; 3

Kuczynski B, Reed B, Mungas D, Weiner M, Chui HC, Jagust W. Cognitive and anatomic contributions of metabolic decline in Alzheimer disease and cerebrovascular disease. Arch Neurol. 2008; 65:650–5. [PubMed: 18474742]

De Leeuw FE, de Groot JC, Achten E, Oudkerk M, Ramos LM, Heijboer R, Hofman A, Jolles J, van Gijn J, Breteler MM. Prevalence of cerebral white matter lesions in elderly people: a population based magnetic resonance imaging study. The Rotterdam Scan Study. J Neurol Neurosurg Psychiatry. 2001; 70:9–14. [PubMed: 11118240]

Li Y, Rinne JO, Mosconi L, Pirraglia E, Rusinek H, DeSanti S, Kemppainen N, Någren K, Kim B-C, Tsui W, de Leon MJ. Regional analysis of FDG and PIB-PET images in normal aging, mild cognitive impairment, and Alzheimer's disease. Eur J Nucl Med Mol Imaging. 2008; 35:2169–81. [PubMed: 18566819]

Lowe VJ, Weigand SD, Senjem ML, Vemuri P, Jordan L, Kantarci K, Boeve B, Jack CR, Knopman D, Petersen RC. Association of hypometabolism and amyloid levels in aging, normal subjects. Neurology. 2014 WNL.0000000000000467–.

Marchant NL, Reed BR, DeCarli CS, Madison CM, Weiner MW, Chui HC, Jagust WJ. Cerebrovascular disease, β-amyloid, and cognition in aging. Neurobiol Aging. 2012; 33:1006, e25–36. [PubMed: 22048124]

Mikheev A, Nevsky G, Govindan S, Grossman R, Rusinek H. Fully automatic segmentation of the brain from T1-weighted MRI using Bridge Burner algorithm. J Magn Reson Imaging. 2008; 27:1235–41. [PubMed: 18504741]

Nordahl CW, Ranganath C, Yonelinas AP, Decarli C, Fletcher E, Jagust WJ. White matter changes compromise prefrontal cortex function in healthy elderly individuals. J Cogn Neurosci. 2006; 18:418–29. [PubMed: 16513006]

Oh H, Habeck C, Madison C, Jagust W. Covarying alterations in Aβ deposition, glucose metabolism, and gray matter volume in cognitively normal elderly. Hum Brain Mapp. 2014; 35:297–308. [PubMed: 22965806]

Palop JJ, Mucke L. Amyloid-beta-induced neuronal dysfunction in Alzheimer's disease: from synapses toward neural networks. Nat Neurosci. 2010; 13:812–8. [PubMed: 20581818]

Provenzano FA, Muraskin J, Tosto G, Narkhede A, Wasserman BT, Griffith EY, Guzman VA, Meier IB, Zimmerman ME, Brickman AM. White matter hyperintensities and cerebral amyloidosis: necessary and sufficient for clinical expression of Alzheimer disease? JAMA Neurol. 2013; 70:455–61. [PubMed: 23420027]

Raj A, Kuceyeski A, Weiner M. A network diffusion model of disease progression in dementia. Neuron. 2012; 73:1204–15. [PubMed: 22445347]

Reed BR, Eberling JL, Mungas D, Weiner M, Kramer JH, Jagust WJ. Effects of white matter lesions and lacunes on cortical function. Arch Neurol. 2004; 61:1545–50. [PubMed: 15477508]

Reisberg B, Sclan S, Franssen E, Deleon M, Kluger A, Torossian C, Shulman E, Steinberg G, Monteiro I, Mcrae T, Boksay I, Mackell J, Ferris S. Clinical stages of normal aging and Alzheimer's disease: The GDS staging system. Neurosci Res Commun. 1993; 13:S51–S54.

Rosenbloom MH, Alkalay A, Agarwal N, Baker SL, O'Neil JP, Janabi M, Yen IV, Growdon M, Jang J, Madison C, Mormino EC, Rosen HJ, Gorno-Tempini ML, Weiner MW, Miller BL, Jagust WJ, Rabinovici GD. Distinct clinical and metabolic deficits in PCA and AD are not related to amyloid distribution. Neurology. 2011; 76:1789–96. [PubMed: 21525424]

Scarpelli M, Salvolini U, Diamanti L, Montironi R, Chiaromoni L, Maricotti M. MRI and pathological examination of post-mortem brains: the problem of white matter high signal areas. Neuroradiology. 1994; 36:393–8. [PubMed: 7936183]

Scheltens P, Barkhof F, Leys D, Wolters EC, Ravid R, Kamphorst W. Histopathologic correlates of white matter changes on MRI in Alzheimer's disease and normal aging. Neurology. 1995; 45:883–8. [PubMed: 7746401]

Sled JG, Zijdenbos AP, Evans AC. A nonparametric method for automatic correction of intensity nonuniformity in MRI data. IEEE Trans Med Imaging. 1998; 17:87–97. [PubMed: 9617910]

Sultzer DL, Chen ST, Brown CV, Mahler ME, Cummings JL, Hinkin CH, Mandelkern MA. Subcortical hyperintensities in Alzheimer's disease: associated clinical and metabolic findings. J Neuropsychiatry Clin Neurosci. 2002; 14:262–9. [PubMed: 12154149]

Tullberg M, Fletcher E, DeCarli C, Mungas D, Reed BR, Harvey DJ, Weiner MW, Chui HC, Jagust WJ. White matter lesions impair frontal lobe function regardless of their location. Neurology. 2004; 63:246–53. [PubMed: 15277616]

Tzourio-Mazoyer N, Landeau B, Papathanassiou D, Crivello F, Etard O, Delcroix N, Mazoyer B, Joliot M. Automated anatomical labeling of activations in SPM using a macroscopic anatomical parcellation of the MNI MRI single-subject brain. Neuroimage. 2002; 15:273–89. [PubMed: 11771995]

Yokokura M, Mori N, Yagi S, Yoshikawa E, Kikuchi M, Yoshihara Y, Wakuda T, Sugihara G, Takebayashi K, Suda S, Iwata Y, Ueki T, Tsuchiya KJ, Suzuki K, Nakamura K, Ouchi Y. In vivo changes in microglial activation and amyloid deposits in brain regions with hypometabolism in Alzheimer's disease. Eur J Nucl Med Mol Imaging. 2011; 38:343–51. [PubMed: 20844871]

Zlokovic BV. Neurovascular pathways to neurodegeneration in Alzheimer's disease and other disorders. Nat Rev Neurosci. 2011; 12:723–38. [PubMed: 22048062]

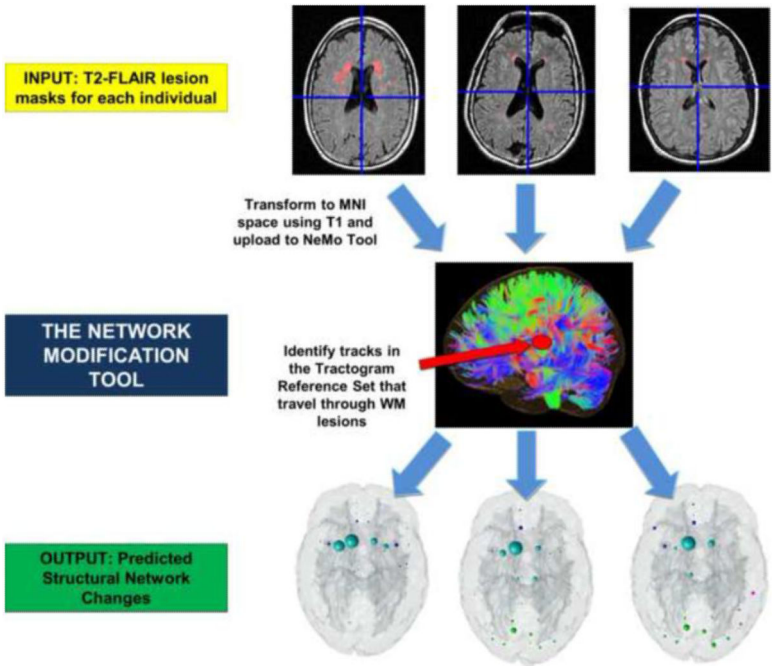

Figure 1. The workflow of image processing

The white matter hyperintensity masks are coregistered to a common space where the Network Modifcation (NeMo) Tool exists. Regional Change in Connectivity (ChaCo) scores, i.e. the percent of tracts connecting to a gray matter region that pass through a white matter hyperintensity, were calculated for each individual.

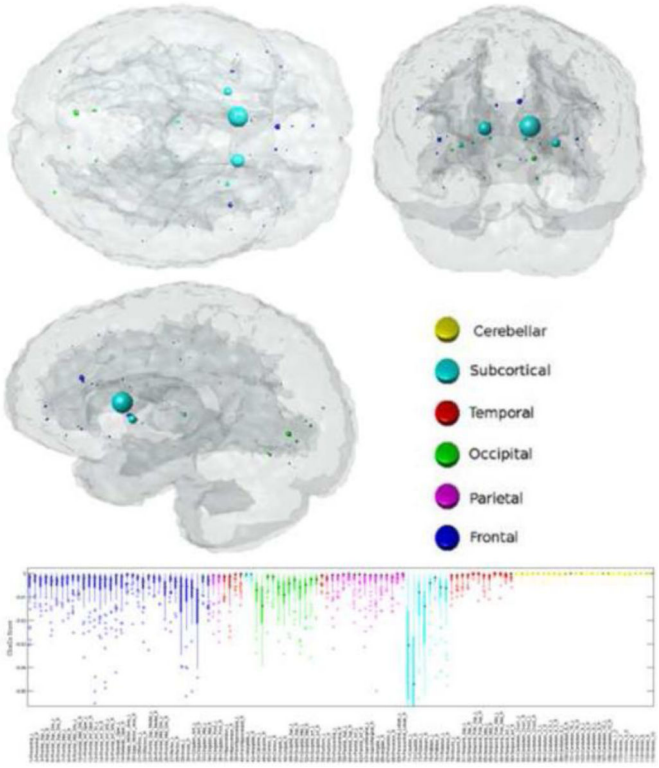

Figure 2. The regional WM disconnection (ChaCo) results

The mean ChaCo over the population is displayed via a glassbrain where each GM region is represented by a sphere whose color denotes regional membership and whose diameter is proportional to its disruption in connection (bigger = more disruption of WM fibers due to WM lesions). The box plot gives the distribution of these scores over the population (color coded with the same key as the glassbrain).

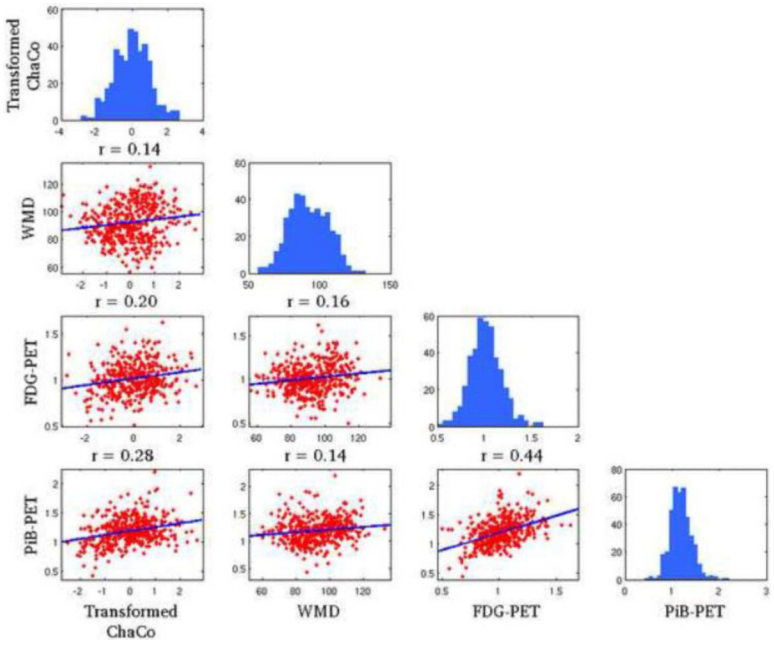

Figure 3. Pearson's correlations of the various imaging biomarkers on a regional basis

Each of the parameters of interest are plotted against one another in the off-diagonal scatter plots and the histograms for each variable are given in the diagonal plots. Correlation values are indicated above each sub-plot.

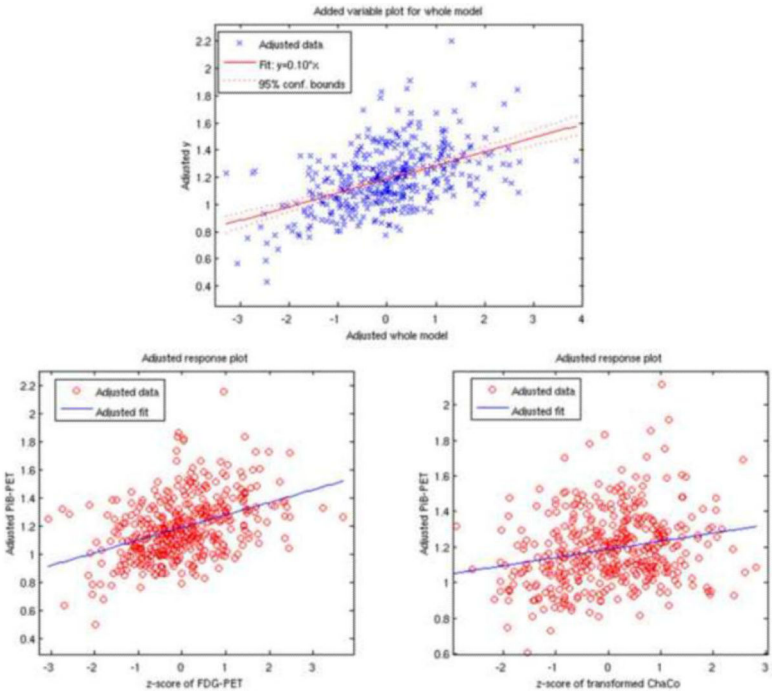

Figure 4. The model resulting from linear regression on a regional basis

PiB-PET was the dependent variable. The top panel gives the predicted versus actual PiB-PET signal, with the two bottom plots showing the adjusted response plots for the two variables included in the final model (FDG-PET and transformed ChaCo).